Front. Environ. Sci. Eng. 2020, 14(4): 69
https://doi.org/10.1007/s11783-020-1248-7

RESEARCH ARTICLE

Photocatalytic water splitting of ternary graphene-like photocatalyst for the photocatalytic hydrogen production

Yan Zhang (✉)[1], Yuyan Zhang[1], Xue Li[1], Xiaohan Zhao[1], Cosmos Anning[1], John Crittenden[2], Xianjun Lyu[1]

1 School of Chemical and Environmental Engineering, Shandong University of Science and Technology, Qingdao 266000, China
2 School of Civil and Environmental Engineering, Georgia Institute of Technology, Atlanta, GA 30332-0595, USA

HIGHLIGHTS

- The MoS_2/SiC/GO composite has a strong photocatalytic activity than SiC.
- The optimal catalyst yielded the highest quantum of 21.69%.
- GO acts as a bridge for electron passage in photocatalytic reaction.

GRAPHIC ABSTRACT

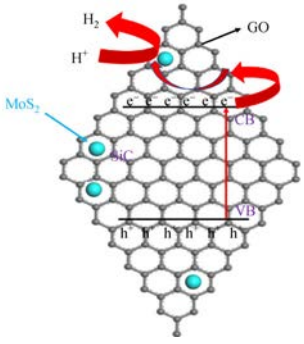

ARTICLE INFO

Article history:
Received 2 September 2019
Revised 21 February 2020
Accepted 12 March 2020
Available online 26 April 2020

Keywords:
Water splitting
Visible light
Graphene-like photocatalyst
Response surface methodology

ABSTRACT

In recent times, there has been an increasing demand for energy which has resulted in an increased consumption of fossil fuels thereby posing a number of challenges to the environment. In the course finding possible solutions to this environmental canker, solar photocatalytic water splitting to produce hydrogen gas has been identified as one of the most promising methods for generating renewable energy. To retard the recombination of photogenerated carriers and improve the efficiency of photocatalysis, the present paper reports a facile method called the hydrothermal method, which was used to prepare ternary graphene-like photocatalyst. A "Design Expert" was used to investigate the influence of the loading weight of Mo and GO as well as the temperature of hydrothermal reaction and their interactions on the evolution of hydrogen (H_2) in 4 h. The experimental results showed that the ternary graphene-like photocatalyst has a strong photocatalytic hydrogen production activity compared to that of pure SiC. In particular, the catalyst added 2.5 wt% of GO weight yielded the highest quantum of 21.69 % at 400–700 nm of wavelength.The optimal evolution H_2 in 4 h conditions was obtained as follows: The loading weight of Mo was 8.19 wt%, the loading weight of GO was 2.02 wt%, the temperature of the hydrothermal reaction was 200.93°C. Under the optimum conditions, the evolution of H_2 in 4 h could reach 4.2030 mL.

1 Introduction

In the current environment, the world faces two major problems: Environmental pollution problems and traditional energy consumption problems (Yuan et al., 2014; Opoku et al., 2017; Yan et al., 2017; Tian et al., 2019). Hydrogen can be one of the greenest and most sustainable energy sources to replace traditional energy sources. It has attracted widespread attention in many fields (Liu et al., 2018a; Liu et al., 2018b; Zhao et al., 2019). In the future environment, the use of energy-intensive and continuous solar-powered semiconductors for photocatalytic water splitting is considered to be one of the most environmentally friendly hydrogen production methods (Li et al., 2019). It can directly convert solar energy into chemical energy, which has solved environmental and energy problems (Shi et al., 2019). As early as 1972, Honda and Fujishima pioneered the photocatalytic water splitting method to produce hydrogen (Fujishima and Honda 1972). Since then, a series of semiconductor materials have been

✉ Corresponding author
E-mail: tougaoktz@163.com

extensively studied for photocatalytic water splitting to produce hydrogen (Chen et al., 2019; Matsubara et al., 2019; Sharma et al., 2019). However, these single photocatalysts have problems such as low photocatalytic hydrogen production activity, low stability, and high cost. Developing a new photocatalyst to solve these problems in order to improve the photocatalytic activity of hydrogen production, suppress the recombination of photogenerated electrons and holes, and improve the scientific problems such as stability.

In the past few decades, Graphene-like photocatalytic materials have been widely studied to improve the photocatalytic activity, owing to their unique structure, high carrier mobility and big specific surface area (Liu et al., 2018c). Graphene-like materials such as Graphene oxide (GO) and molybdenum disulfide (MoS_2) are used in the preparation of photocatalytic materials and their superior properties are used to modify the main photocatalyst. Recently, MoS_2 has been reported to be an excellent co-catalyst for photocatalytic hydrogen evolution (Jiang et al., 2019; Wang et al., 2019). For example, Hao et al. (2019) studied $MoS_2/ZnIn_2S_4$ composites with MoS_2 anchored on the surface of $ZnIn_2S_4$ microspheres by a two-step hydrothermal process that exhibited significantly enhanced photocatalytic H_2 evolution than pure $ZnIn_2S_4$ (Hao et al., 2019). Benavente et al. (2018) synthesized hetero structured layered hybrid ZnO/MoS_2 nanosheets to enhance visible light photocatalytic activity (Benavente et al., 2018). It has been commonly known, that the facilitation of the photocatalytic H_2 evolution using MoS_2 as a co-catalyst originates from the unsaturated edge sulfur atoms, which act as an active site (Peng et al., 2019).

Silicon carbide (SiC) ranging from 2.7 eV to 3.2 eV has been deemed as one of the most promising photocatalytic because it acts as a graphene-like material, good physical and chemical properties. Wang et al. (2017a) used an in situ heating thiourea method to prepare g-C_3N_4/SiC composites (Wang et al., 2017a). Their Photocatalytic experimental results showed that, the g-C_3N_4/SiC composites exhibited high stability in H_2 production and also demonstrated a maximum of 182 μmol/g/h. Yuan's group spatially separated Pt and IrO_2 deposition on the micro-SiC surface via an in situ photodepositing method (Wang et al., 2017b). They achieved a H_2 evolution of robustly 70.1 μL in 3 h in the presence sacrifice reagent.

Considering the excellent physical and chemical properties of GO and MoS_2, we report a simple and economical approach that combines the advantages of GO and MoS_2 to improve the photocatalytic activity of MoS_2/SiC/GO (SMG) composite significantly. Base on this, we synthesized SMG composite by a hydrothermal synthesis method and researched its photocatalytic activity and the rate of H_2 evolution. Moreover, the enhancing photocatalytic activity mechanism of SMG composite has been discussed.

2 Materials and methods

2.1 Materials

The materials used in this experiment are as follows: SiC powders (Shanghai Macklin Biochemical Co., Ltd., China), Molybdenum disulfide (MoS_2, Shandong West Asia Chemical Co., Ltd., China), Graphene (GO, Tanfeng Tech. Inc., China), an ionic liquid (1-butyl-3-methylimidazolium hexafluorophosphate, Shanghai Chengjie Chemical Co., Ltd., China).

2.2 Photocatalyst synthesis

Prior to its usage, the SiC powder was pretreated as described in our previous paper (Zhang et al., 2019). A series of MoS_2/SiC/GO photocatalysts were synthesized using the following procedure: first, 0.7769 g of MoS_2 was dissolved in 100 mL of DI water. Second, 0.1178 g of GO and 5 g of pure SiC particles were added to the suspension and then the resultant solution was ultrasonicated for 4 h. Continue adding 2 drops of ionic liquid ([BMIM] PF_6) and continue sonication for 6h. Then, the mixed solution was subjected to a hydrothermal reaction at 200°C for 20 h using a 300 mL Teflonlined stainless-steel autoclave.After the solution was allowed to cool to room temperature, it was then centrifuged and washed with deionized water until the pH 7. After, the samples were dried at 60°C overnight in a vacuum environment and grounded into the particle denoted as SMG-2, indicating an added weight percent of 2 wt% GO. The loading weight percentage of 2.0 wt% of GO was based on the total co-catalyst and SiC mass. For comparison, SiC/G-2.5 (Mass concentration of GO is 0.5872 g in composites)was conducted in the same condition. For obtaining different MoS_2/SiC/GO composites, when the loading weight percent of Mo was 0.7769 g, the loading weight percent of GO was changed to 1 wt%, 1.5 wt%, 2 wt%, 2.5 wt%, and 3 wt%, defined as SMG-1, SMG-1.5, SMG-2, SMG-2.5, and SMG-3 respectively. ICP-AES analysis was used to determine the Mo loading in the samples and the average value was 7.866 mg/L.

2.3 Characterization

Inductively, coupled plasma-atomic emission spectrometer (ICP-AES) were conducted using Agilent icpoes730 to determine the accurate loading of MoS_2. Scanning electron microscopy (SEM) and energy disperse spectroscopy (EDS) analysis was performed using APREO scanning electron microscope. In obtaining the patterns, a diffractometer was used. The conditions under which powder X-ray diffraction (XRD, a Rigaku Ultima IV) with the use of Cu Kα radiation is tested are 2θ range of 30° to 80° and 4° per minute scanning speed.The BET specific surface area

was measured using a Micromeritics ASAP 2460 instrument. The UV-visible diffuse reflectance (DRS, UH4150, Hitachi) was used to measure the absorption spectral range of the composite catalyst.This instrument used $BaSO_4$ as the reflectance standard.The ESCALAB 250Xi X-ray Photoelectron Spectrometer (XPS) was used for further validation of the samples using Al Kα radiation.

2.4 Photocatalytic H_2 reaction

Details of the photocatalytic reactor is described in our previous article (Zhang et al., 2019). 0.5 g of the sample was dispersed in 100 mL sacrificial agent with 1M $Na_2S{\cdot}9H_2O$, 1M Na_2SO_3 (Yan et al., 2009). The mixed solution was adjusted to pH 7. After passing N_2 for 30 min, the N_2 valve was closed. The reactor was continuously stirredat 400 r/min and the photocatalytic system was irradiated with a 400–700 nm Xe lamp. Gas was then collected. The hydrogen was analyzed by gas chromatography (GC-9790 II, TCD) with argon as the carrier gas. The photocatalytic activity of the catalyst was evaluated using a photocatalytic H_2 production rate in 4 h.

The rate of H_2 production in 4 h was calculatedwith the aid of Eq. (1):

$$r_m = \frac{n}{t \times m} \tag{1}$$

The QY is defined by the following Eqs. (2)–(5) (Zhang et al., 2013; Zhang et al., 2014) was calculatedby a band-pass interference filter ($\lambda = 400$–700 nm) and the spectro-radiometer:

$$\mathrm{QY} = \frac{r \times 2}{N} \times 100\% \tag{2}$$

$$N = S \times I \tag{3}$$

$$I = \int_{\lambda_2}^{\lambda_1} R d\lambda \tag{4}$$

$$r = \frac{n}{t} \tag{5}$$

The detailed description of two formulas are indicated in our previous article (Zhang et al., 2019).

2.5 Experimental design using Box–Behnken

Based on a single experimental factor, the influence of various factors on H_2 evolution in 4 h was considered synthetically. The H_2 evolution in 4 h was optimized and the experimental result of photocatalytic water splitting reaction was regression fitted with a quadratic polynomial to predict the best conditions of photocatalytic water splitting, according to Box-Behnken and Design Expert (Yu et al., 2018; Zhang et al., 2018). The H_2 evolution in 4 h by photocatalyst was considered as a response (Y). The loading weight percent of Mo(A), the loading weight of GO(B) and the temperature of the hydrothermal reaction (C) were used as independent variables. Table 1 shows the design levels and parameters. Table 2 shows the design and experimental results.

Table 1 Symbols and coded

Variables	Symbol	Code levels		
		–1	0	1
Loading weight of Mo (wt%)	A	2	6	10
Loading weight of GO (wt%)	B	1	2	3
Temperature of hydrothermal reaction (°C)	C	180	200	220

Table 2 Design and experimental results

Run	Coded values			H_2 evolution in 4 h (mL)
	A	B	C	
1	–1	–1	0	3.8132
2	0	0	0	4.2757
3	0	0	0	4.2757
4	–1	0	–1	3.7989
5	0	0	0	4.2757
6	–1	1	0	3.8149
7	1	–1	0	3.8146
8	0	–1	–1	3.8268
9	–1	0	1	3.8194
10	1	0	–1	3.8002
11	0	1	1	3.8757
12	0	0	0	4.2757
13	0	0	0	4.2757
14	1	0	1	3.8412
15	1	1	0	3.8329
16	0	1	–1	3.8311
17	0	–1	1	3.8594

3 Results and discussion

3.1 Electron microscopy

Figures 1 and S1(in the supporting materials) revealed that the morphologies of the prepared pure SiC, MoS_2/SiC/GO catalytic and SMG-2.5 catalyst after circular reaction (defined as SMG-C2.5) by scanning electron microscopy (SEM). Figures 1(a), 1(b) and 1(g) are the SEM images of pure SiC, SMG-2.5, and SMG-C2.5, respectively. As seen from Fig. 1(a), the prepared pure SiC materials were sheet structures. Figures S1(a–d) are the SEM images of SMG-1, SMG-1.5, SMG-2, and SMG-3, respectively. The prepared

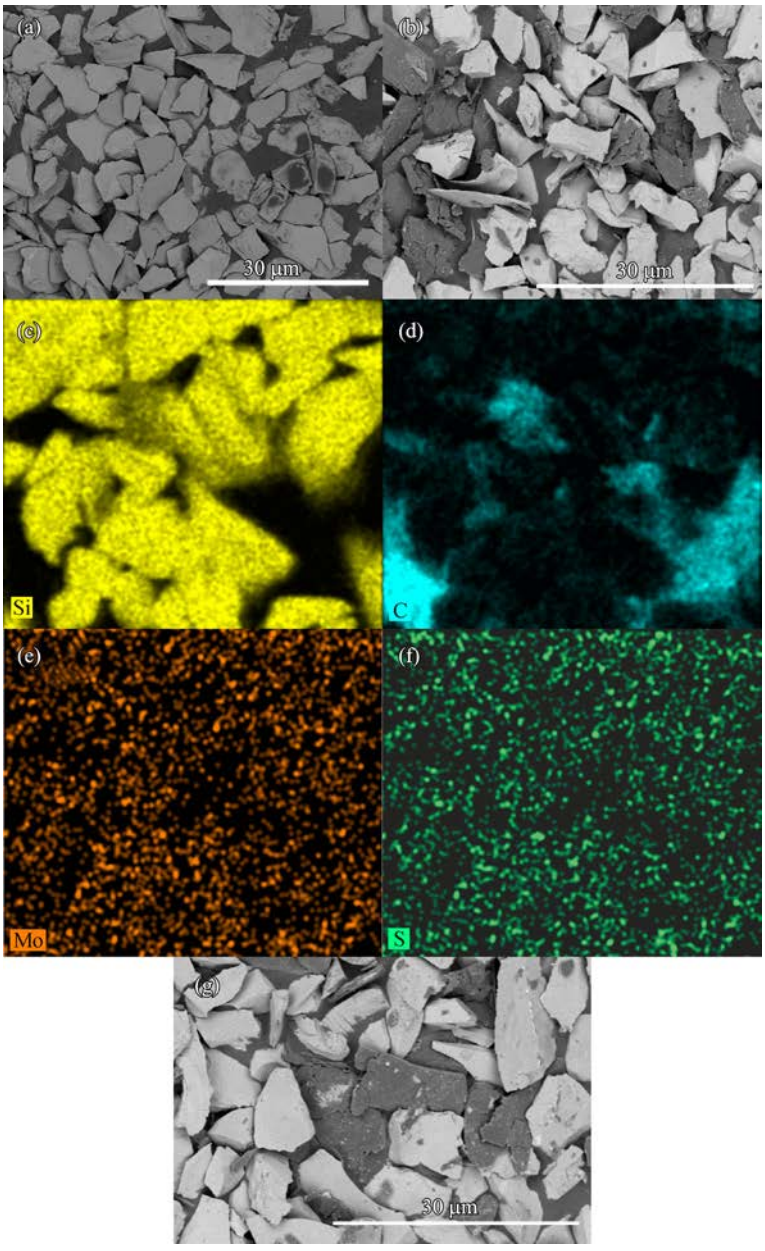

Fig. 1 SEM image of (a) pure SiC, (b) SMG-2.5 and element mapping images SMG-2.5 (c–f), (g) SMG-2.5 catalyst after circular reaction (SMG-C2.5).

MoS_2/SiC/GO composites were sheet structures that were the same as the pure SiC. MoS_2 and GO are randomly dispersed in the intermediate layer between SiC and have good contact with each other. In addition, there are more contact surfaces between the three SMG-2.5 composite catalysts. It can be inferred that the contact surfaces provide more reactive sites for photocatalytic hydrogen production. Element mapping (EDS) of SMG-2.5 (Fig. 1 (c–f)) reveals that Si, C, Mo and S elements are distributed in an entire composites. These structural analysis results have proven that GO and MoS_2 effectively built into the pure SiC. Compared with SMG-2.5, the sheet structure of SMG-C2.5 has not changed significantly. It shows that the structure of the sample after the photocatalytic reaction has not changed.

3.2 Crystallinity analysis

The crystalline structure of the prepared samples were investigated using XRD. Fig. 2 (a) shows the XRD patterns of SMG-x (x = 1, 1.5, 2, 2.5, 3), pure SiC and SMG-C2.5. Despite the difference in x values, the XRD patterns of these photocatalysts were similar, which showed that the x values have a negligible effect on the crystallinity. We

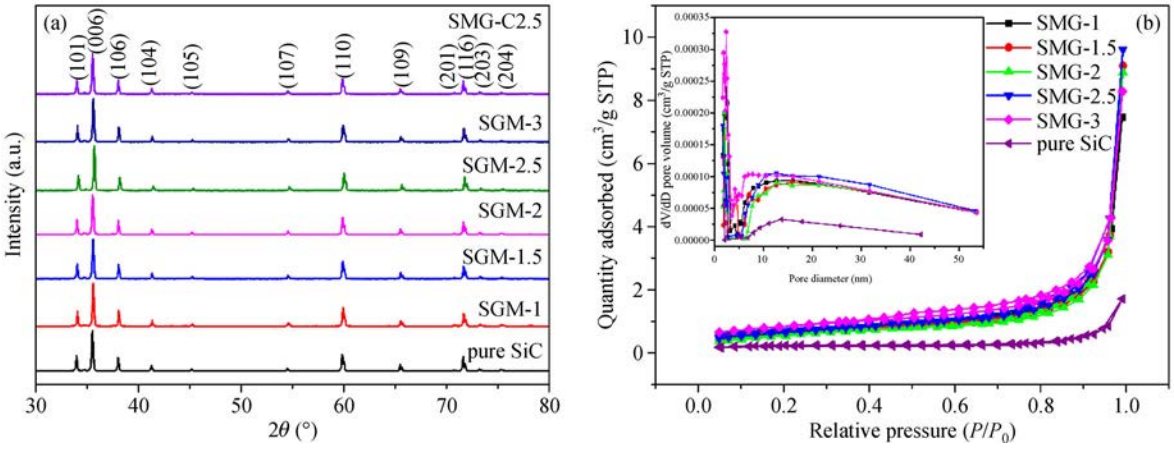

Fig. 2 (a) XRD patterns, (b) nitrogen adsorption-desorption isotherms and the pore-size distribution curves (inset).

observed that there were 12 diffraction peaks at 2θ = 34.097°, 35.658°, 38.136°, 41.392°, 45.294°, 54.630°, 60.010°, 65.626°, 70.856°, 71.765°, 73.358°, and 75.520° assigning to (101), (006), (103), (104), (105), (107), (110), (109), (201), (116), (203) and (204) planes of 6H-SiC (JCPDS card # 72-0018) respectively (Wang et al., 2015). The XRD patterns of the MoS_2/SiC/GO photocatalyst indicated that it has a similar structure to that of pure SiC. This shows that GO has no significant effect on the crystal structure of 6H-SiC during the hydrothermal process and has not been trapped inside the lattice of 6H-SiC. Moreover, no peak of GO has been reflected in XRD patterns, which may be due to the low contents and high dispersion of GO in these samples (Yuan et al., 2015). Interestingly, it was also found that the intensity of this (006) peak in composite photocatalysts significantly increases as compared to that of pure SiC. This may be possible due to the fact that GO changes the crystallinity of SiC. In comparison, the diffraction peaks and peak intensities of SMG-C2.5 did not change significantly. This indicates that the crystal structure of the sample has not changed after the cyclic reaction.

3.3 Textural properties

The specific surface area and pore size of the synthesized GO/SiC/MoS_2 composites were determined by the nitrogen adsorption-desorption isotherm. Figure 2(b) shows the adsorption-desorption isotherms and pore size distributions (the inset) for pure SiC, SMG-1, SMG-1.5, SMG-2, and SMG-3, respectively. According to the IUPAC classification, the isotherms of samples show that the typical type IV has an H3 type hysteresis loop as shown in Fig. 2(b). This indicates the presence of mesopores (Yuan et al., 2015). Table S1 (in the Supporting materials) shows the BET specific surface area and pore size of all the samples. Compared with pure SiC, the specific surface area of the composite sample becomes larger, which can be ascribed to the role of GO and MoS_2. The pore size distribution diagram (inset) showed that the pore size of the composite catalyst is mainly distributed at 10–40 nm.

3.4 UV-visible absorption spectra

The optical properties of pure SiC, MoS_2, and its composites were determined using the UV-vis diffuse reflectance spectra. Figure 3(a) depicts the UV-vis absorption spectra of the prepared samples. MoS_2 itself has no photocatalytic activity because its forbidden bandwidth and the position of the conduction band valence do not meet the requirements for photocatalytic water decomposition. Apparently, the spectra of SMG-1, SMG-1.5, SMG-2, SMG-2.5, and SMG-3 are quite different from pure SiC. Compared with pure SiC, the absorption intensities of all the composites samples are obviously larger in the vis-light region. The bandgap energy of the samples was calculated using Eq. (6) based on Tauc's Equation (Nowak et al., 2009; Zhao et al., 2018):

$$(Ahv)^2 = K(hv - E_g) \tag{6}$$

where *Eg* stands for the bandgap energy; hv stands for photon energy; *K* and *A* represent proportionality constant and absorption coefficient, respectively.

The normalized graphs of $(Ahv)^2$ for the photon energy of the samples are shown in Fig. 3(b) and the bandgap energy of all samples is shown in Table S1 (in the Supporting materials). Compared with the pure SiC UV-vis DRS, the composite samples showed enhanced photoabsorption in the wavelength range from 370 to 770 nm caused by the strong photoabsorption of the MoS_2/GO, and the composites have a significant degree of redshift. Compared with pure SiC, the bandgap energies of all the composites samples decreased significantly and are between 1.94 and 2.08 eV. The forbidden bandwidth of SMG-2.5 is 1.94 eV, and the photocatalytic hydrogen

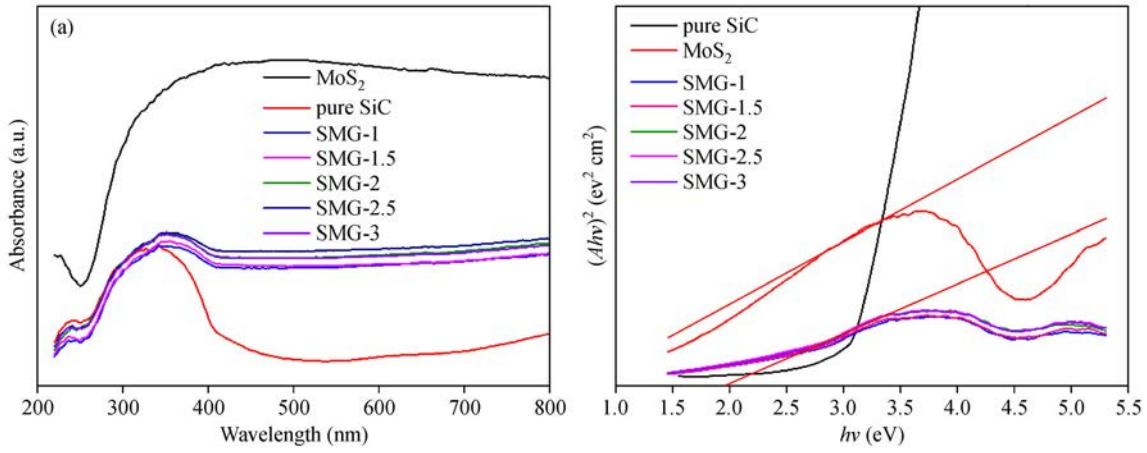

Fig. 3 (a) UV-vis diffuse reflectance spectra and (b) Corresponding Tauc plots.

production performance is the best. This shows that the light absorption performance of the MoS_2/SiC/GO composite catalyst can be adjusted microscopically so that it can effectively absorb visible light for photocatalytic hydrogen production. The decreasing bandgap suggests that incorporating GO and MoS_2 in SiC particles can effectively reduce its bandgap into the visible-light absorption region.

3.5 X-ray photoelectron spectrometer

XPS is further used to verify the successful preparation of MoS_2/SiC/GO composites and examine the valence state of C, Si, Mo and S element. Fig. 4 shows XPS results of pure SiC and SMG-2.5. VB-XPS plots tests of SiC and MoS_2 are shown in Figs. 4(g) and 4(h). As seen from Figs. 4(a) and 4(b), the C 1s spectrum shows two binding energy(BE) peaks at 282.9 and 284.6 eV, which are associated with C-Si and C-C, respectively (Zhang et al., 2019). Compared with pure SiC, the peak area of the C-C bond of SMG-2.5 is enhanced.The Si 2p spectrum is shown in Figs. 4(c) and 4(d). The Si 2p spectrum shows the peaks of two BE at 100.8 and 102.1 eV which are associated with Si–C and Si–O bonds, respectively (Zhang et al., 2019). The Mo 3d and S 2p spectrum of SMG-2.5 samples are shown in Figs. 4(e) and 4(f). As seen from Fig. 4(e), the Mo $3d_{5/2}$ and Mo $3d_{3/2}$ peaks of the binding energy are 228.9 and 232.5 eV, respectively (Lv et al., 2017; Zhao et al., 2017). The results indicate the presence of Mo^{4+} (Yin et al., 2016). The peak of binding energy of approximately 226.3 eV indicates the presence of 2s orbital interaction of S. The peaks of the binding energy (BE) of approximately 233.1 and 230.6 eV indicate the presence of Mo^{5+} (Zhang et al., 2019). The peak of binding energy of approximately 235.7eV indicates the presence of Mo^{6+} (Jiang et al., 2018). This indicates that the presence of MoS_2/SiC/GO composite the two peaks at binding energies 161.3 and 163.3 eV and correspondsto S $2p_{3/2}$ and S $2p_{1/2}$ which represents the presence of S^{2-} (Fig. 4f) (Heydari-Bafrooei and Shamszadeh 2016). From Figs. 4(g) and 4(h), the position of the valence band top of SiC is 1.2 eV, and the position of the valence band top of MoS_2 is 0.2 eV.

3.6 Photocatalytic activity and stability

The photocatalytic activities and stability of samples were measured in Fig. 5. The hydrogen production result of photocatalyst in 4 h are shown in Fig. 5(a). The H_2 production of SMG-1, SMG-1.5, SMG-2, SMG-2.5, SMG-3, and SiC/G-2.5 showed 2.7876 mL, 2.8410 mL, 3.21 mL, 4.5297 mL, 3.0679 mL, and 2.5212 mL, respectively. For comparison, the average photocatalytic H_2 evolution rates in 4 h are calculated and shown in Fig. 5(b). The average rates of hydrogen generation were determined to be 56.89 μmol/g/h, 57.98 μmol/g/h, 65.51 μmol/g/h, 92.44 μmol/g/h, 62.61 μmol/g/h, and 51.45 μmol/g/h for SMG-1, SMG-1.5, SMG-2, SMG-2.5, SMG-3, and SiC/G-2.5, respectively. Obviously, all of the photocatalysts exhibited better photocatalytic activities than the pure SiC, especially the weight loading of 2.5 wt% GO onto the SiC/MoS_2 composites could achieve the highest H_2 evolution rate. The catalyst added 2.5 wt% of GO weight yielded the highest quantum of 21.69% at 400–700 nm of wavelength. The result indicates that GO can effectively improve the photocatalytic activity and the loading weight of GO is also important for photocatalytic hydrogen production. The case where the content of GO is higher but its photocatalytic hydrogen production performance is low, excessive GO will increase photon absorption and scattering during the photocatalytic reaction. The photocatalytic stability of the samples is also crucial for its practical application. Thus, the long-term photocatalytic stability and reproducibility of the photocatalyst samples for H_2 generation were further evaluated through three consecutive runs under the same

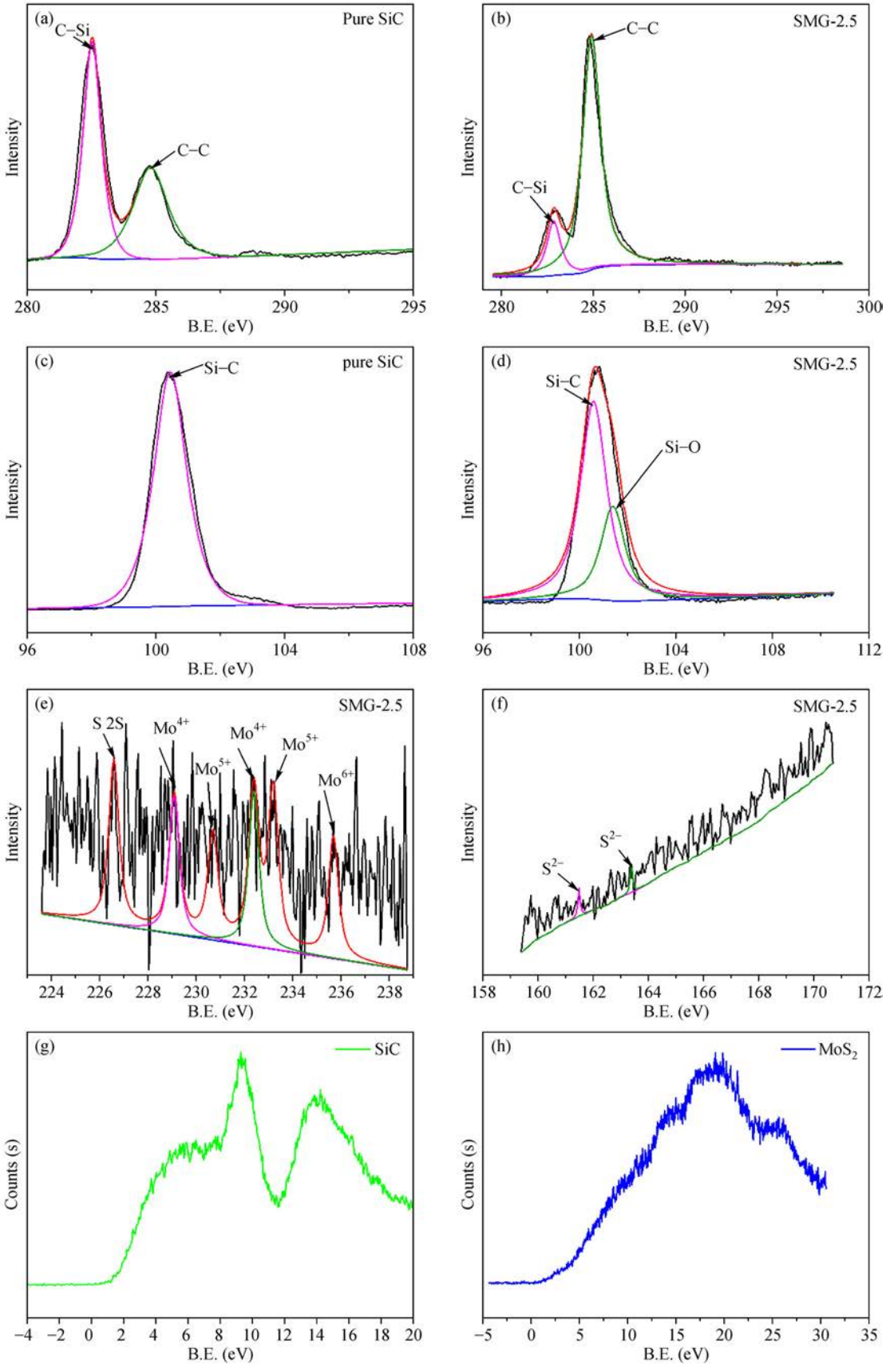

Fig. 4 XPS spectra of (a) C 1s of pure SiC, (b) C 1s of SMG-2.5, (c) Si 2p of pure SiC, (d) Si 2p of SMG-2.5, (e) Mo 3d and (f) S 2p in SMG-2.5 sample, (g) VB-XPS of SiC, (h) VB-XPS of MoS_2.

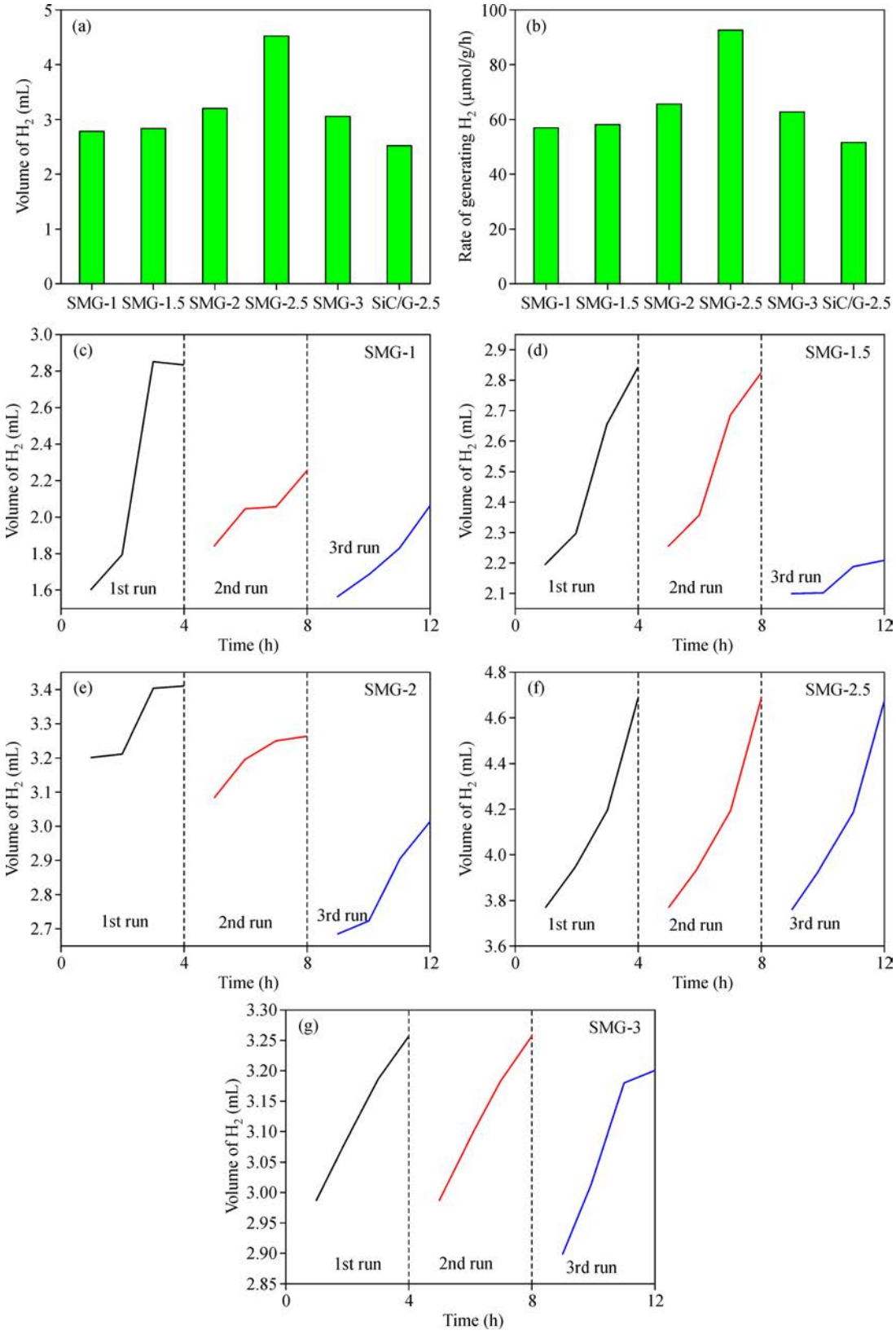

Fig. 5 (a) Volume of H_2 in 4 h over the composites. (b) Rate of generating H_2 in 4 h over composites. (c)–(g) Recycling H_2 evolution tests over MoS_2/SiC/GO composites.

conditions. Each cycle was performed under the same light irradiation condition for 4 h. The reaction system was re-evacuated, after each run. Figs. 5(c)–5(f) display the cycling measurements of photocatalytic H_2 generation over all the samples under visible light irradiation(400–700 nm). As seen from Figs. 5(c)–5(f), the photocatalytic stability of the SMG-2.5 sample was excellent after three consecutive experiments. The result indicates that proper GO loading can enhance the photocatalytic hydrogen generation activity and maintain good stability of photocatalytic hydrogen generation.

3.7 Analysis of response surface design of the H_2 evolution in 4 h

3.7.1 Model equation construction

The effect of key factors such as the loading weight of Mo, the loading weight of GO, the temperature of the hydrothermal reaction, and their interactions were investigated for photocatalytic water splitting for H_2 evolution in 4 h. The H_2 evolution in 4 h experimental data by MoS_2/SiC/GO photocatalyst in Table 2 was analyzed using software Design-Expert 8.0 software by quadratic regression fitting (Yu et al., 2018).

The design includes 17 runs to evaluate the error between each test by considering five replicates. In this design, the related factor or interaction isoutstanding. Hence, parameters A, B, and C and their interactions (i.e. AB, AC, BC, A^2, B^2, and C^2) for the H_2 evolution in 4 h are significantly considerable. Meantime, quadratic multinomial regression Eq. (7) were got by OPTIMIZATION of "Design Expert" to study the influence of the experimental variables on the photocatalytic water splitting for H_2 evolution in 4 h:

$$\begin{aligned} H_2 \text{ evolution (mL)} &= 4.27 + 5.563 \times 10^{-3}\mathrm{A} \\ &+5.075 \times 10^{-3}\mathrm{B} + 0.017\mathrm{C} + 4.15 \times 10^{-3}\mathrm{AB} \\ &+4.625 \times 10^{-3}\mathrm{AC} + 3 \times 10^{-3}\mathrm{BC} - 0.24A^2 \\ &-0.21B^2 - 0.21C^2 \end{aligned} \quad (7)$$

The model F-value represents the mean square ratio between the groups in the ANOVA analysis. It can reflect the importance of each factor for the H_2 evolution in 4 h and is used to evaluate the observability of the fitted model (Delavari and Amin 2014). With regards to Table 3, the Model F-value of 12662.57 indicates that the model is important.

Use Eq.(7) to construct the contour map with the third independent variable at the midpoint level (Zhou et al., 2018). Equation (7) indicates that the evolution of H_2 in 4 h efficiency improved with a loading weight of Mo usage (A), loading weight of GO(B) and temperature of hydrothermal reaction(C).

In this work, A, B, C, AB, AC, BC, A^2, B^2, C^2 are important model terms. The ANOVA was adopted to assess the significance of the developed model. In this work, the "Pred R-Squared" of 0.9990 is in reasonable agreement with the "Adj R-Squared" of 0.9999. These results indicate that the prediction model can well describe the evolution of H_2 in 4 h behavior.

3.7.2 3D response surface and contour plots

Contour plots (Fig. 6) present the interaction of each independent actor on the response variables in the whole design space (Koh et al., 2017; Bazrafshan et al., 2019).

Table 3 Regression model and variance analysis

Source	Sum of Squares	df	Mean Square	F value	Prod>F
Model	0.71	9	0.078	12662.57	< 0.0001
A	2.475×10^{-3}	1	2.475×10^{-3}	40.05	0.0004
B	2.060×10^{-3}	1	2.060×10^{-3}	33.33	0.0007
C	2.336×10^{-3}	1	2.336×10^{-3}	377.91	< 0.0001
AB	6.889×10^{-4}	1	6.889×10^{-4}	11.15	0.0124
AC	8.556×10^{-4}	1	8.556×10^{-4}	13.84	0.0075
BC	3.600×10^{-4}	1	3.600×10^{-4}	5.82	0.0465
A^2	0.25	1	0.25	40294.37	< 0.0001
B^2	0.19	1	0.19	30151.75	< 0.0001
C^2	0.19	1	0.19	31156.01	< 0.0001
Pure Error	0	4	0		
Cor Total	0.71	16			

Note: A, B, and C represent variables of the loading weight of Mo, the loading weight of GO, and the temperature of the hydrothermal reaction, respectively.

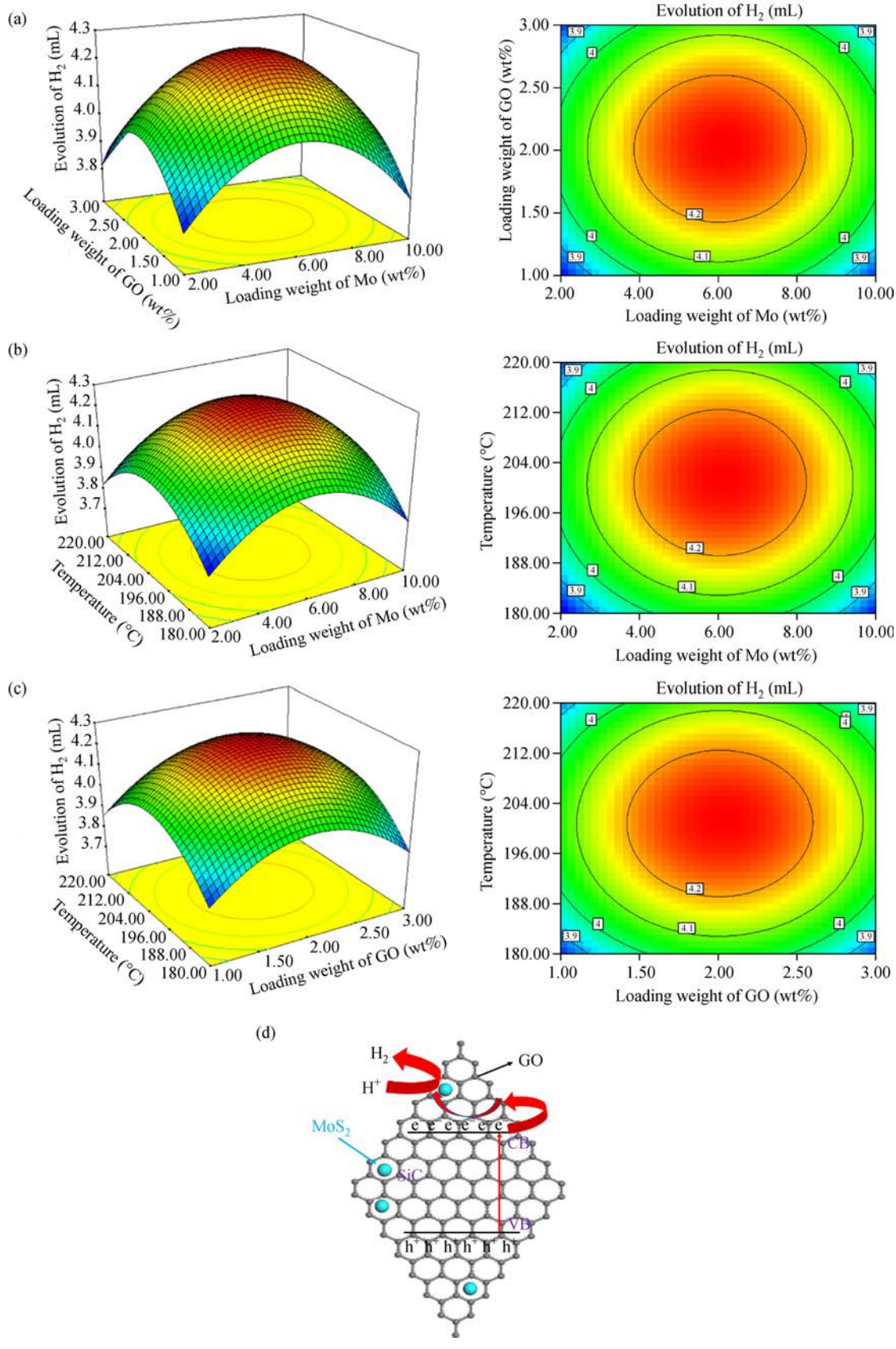

Fig. 6 3D response surface and contour plots of the H_2 evolution in 4 h: (a) loading weight of Mo and loading weight of GO, (b) loading weight of Mo and temperature of the hydrothermal reaction, (c) loading of GO and temperature of the hydrothermal reaction, (d) the photocatalytic hydrogen production mechanism in the MoS_2/SiC/ GO photocatalyst.

The effects of loading weight of Mo, loading weight of GO, and temperature of hydrothermal reaction on the evolution of H_2 in 4 h are plotted in Figs. 6(a–c).

The results revealed that there are optimal three independent variables for 4 h of hydrogen production. Meanwhile, the effect of temperature of the hydrothermal reaction is much more obvious than the loading weight of Mo and GO on the evolution of H_2 in the 4 h process. Based on the results of ANOVA and the construction of the model equation, the optimal conditionswere considered to be 8.19 wt% Mo, 2.02 wt% GO, and hydrothermal reaction at 200.95°C. At this point, the evolution of H_2 in 4 h may reach 4.2030 mL. Furthermore, the shape of the relationship between these factors implies the strength of the interaction between the variables. That is, the circular contours indicate a weaker interaction intensity (Muthukumar et al., 2017). Thence, Figures 6(a–c) show that the interaction intensity of each other is almost the same.

3.7.3 Verification of optimal conditions

To verify the prediction of the optimal conditions, three sets of parallel experiments were performed under the optimal conditions required to compare the hydrogen yield obtained from the test with the predicted results. We re-prepared a new sample under the following conditions; the loading weight of Mo was 8.19 wt%, the loading weight of GO was 2.02 wt% and the temperature of the hydrothermal reaction was 200.93°C. Three samples (4.1026 mL, 4.2107 mL, and 4.1098 mL) were prepared and kept for 4 h for photocatalytic hydrogen production. The average of the hydrogen production in 4 h is 4.1410 mL. The error of the test average is 1.47%, and the prediction result is good. To verify the optimal reaction conditions of the prepared materials obtained by the Design-Expert software, experiments were performed to confirm the given conditions.

3.8 Mechanism for H_2 Evolution

Based on the above studies, it can be confirmed from Fig. 6(d) that the mechanism of photocatalytic H_2 in the GO/SiC/MoS_2 system with GO/MoS_2 as co-catalyst is due to the synergistic effect of MoS_2 and GO. The cocatalyst is effectively improved by the photocatalytic activity of GO/SiC/MoS_2 photocatalyst, the electron-hole separation efficiency, and the transfer efficiency. Under visible light, the photogenerated electrons of SiC are excited and transferred to the surface of SiC. The electrons of SiC can be transferred to MoS_2 through graphene, and hydrogen is generated by reaction with H^+ under visible light irradiation. GO acts as an intermediate bridge. The electrons generated by the SiC are transferred to the MoS_2 by GO, and the hydrogen is generated by reacting with H^+ under visible light irradiation.

4 Conclusions

In conclusion, ternary graphene-like photocatalysts were successfully synthesized by a one-step hydrothermal method. This study demonstrated that the ternary photocatalyst possessed higher photocatalytic activity for hydrogen evolution and promoted the separation of photogenerated electron-hole pairs than pure SiC and binary composite photocatalysts. In particular, the SMG-2.5 shows a significant increase in the average rate of hydrogen evolution in 4 h as compared to the pure. This reveals that graphene-like materials as cocatalysts improve the photocatalytic hydrogen production activity of SiC. This research not only provides an excellent candidate for photocatalytic hydrogen production but also provideda facile method approach to explore highly efficient ternary graphene-like semi-conductor photocatalyst for photocatalytic H_2 generation. According to Box-Behnken, a quadratic model was designed to predict the change of hydrogen production in 4 h. It can be seen from the predicted quadratic model that with the loading weight of Mo and GO and the increase of hydrothermal reaction temperature, the evolution of 4 h efficiency H_2 increases and then decreases. The optimum solution suggested by OPTIMIZATION of "Design Expert" was 8.19 wt% Mo, 2.02 wt% GO, and 200.93°C with 4.2030 mL H_2 evolution.

Acknowledgements The financial was supported by the National Natural Science Foundation of China (Grant No. 51674161), Innovation Team Project of Shandong University of Science and Technology (No. 2012KYTD102), Specialized Research Fund for the Doctoral Program of Higher Education (No. 20133718110005), and Shandong Provincial Education Association for International Exchanges is gratefully acknowledged. Also, the authors gratefully acknowledge support from the Brook Byers Institute for Sustainable Systems, Hightower Chair and the Georgia Research Alliance at the Georgia Institute of Technology.

Electronic Supplementary Material Supplementary material is available in the online version of this article at https://doi.org/10.1007/s11783-020-1248-7 and is accessible for authorized users.

References

Bazrafshan E, Al-Musawi T J, Silva M F, Panahi A H, Havangi M, Mostafapur F K (2019). Photocatalytic degradation of catechol using ZnO nanoparticles as catalyst: Optimizing the experimental parameters using the Box-Behnken statistical methodology and kinetic studies. Microchemical Journal, 147: 643–653

Benavente E, Durán F, Sotomayor-Torres C, González G (2018). Heterostructured layered hybrid ZnO/MoS_2 nanosheets with enhanced visible light photocatalytic activity. Journal of Physics and Chemistry of Solids, 113: 119–124

Chen H, Tan C, Zhang K, Zhao W, Tian X, Huang Y (2019). Enhanced photocatalytic performance of ZnO monolayer for water splitting via

biaxial strain and external electric field. Applied Surface Science, 481: 1064–1071

Delavari S, Amin N A S (2014). Photocatalytic conversion of carbon dioxide and methane over titania nanoparticles coated mesh: Optimization study. Energy Procedia, 61: 2485–2488

Fujishima A, Honda K (1972). Electrochemical photolysis of water at a semiconductor electrode. Nature, 238(5358): 37–38

Hao M, Deng X, Xu L, Li Z (2019). Noble metal free $MoS_2/ZnIn_2S_4$ nanocomposite for acceptorless photocatalytic semi-dehydrogenation of 1,2,3,4-tetrahydroisoquinoline to produce 3,4-dihydroisoquinoline. Applied Catalysis B: Environmental, 252: 18–23

Heydari-Bafrooei E, Shamszadeh N S (2016). Synergetic effect of CoNPs and graphene as cocatalysts for enhanced electrocatalytic hydrogen evolution activity of MoS_2. RSC Advances, 6(98): 95979–95986

Jiang Q, Sun L, Bi J, Liang S, Li L, Yu Y, Wu L (2018). MoS_2 quantum dots modified covalent triazine-based frameworks for enhanced photocatalytic hydrogen evolution. ChemSusChem, 11(6): 1108–1113

Jiang Y, Wang Q, Han L, Zhang X, Jiang L, Wu Z, Lai Y, Wang D, Liu F (2019). Construction of In_2Se_3/MoS_2 heterojunction as photoanode toward efficient photoelectrochemical water splitting. Chemical Engineering Journal, 358: 752–758

Koh P W, Yuliati L, Lee S L (2017). Kinetics and optimization studies of photocatalytic degradation of methylene blue over Cr-doped TiO_2 using response surface methodology. Iranian Journal of Science & Technology Transactions A Science: 1–9

Li Z, Hou J, Zhang B, Cao S, Wu Y, Gao Z, Nie X, Sun L (2019). Two-dimensional Janus heterostructures for superior Z-scheme photocatalytic water splitting. Nano Energy, 59: 537–544

Liu J, Ke J, Li Y, Liu B, Wang L, Xiao H, Wang S (2018b). Co_3O_4 quantum dots/TiO_2 nanobelt hybrids for highly efficient photocatalytic overall water splitting. Applied Catalysis B: Environmental, 236: 396–403

Liu X, Chen C, Chen X, Qian G, Wang J, Wang C, Cao Z, Liu Q (2018c). WO_3 QDs enhanced photocatalytic and electrochemical perfomance of GO/TiO_2 composite. Catalysis Today, 315: 155–161

Liu Y, Yang S, Zhang S, Wang H, Yu H, Cao Y, Peng F (2018a). Design of cocatalyst loading position for photocatalytic water splitting into hydrogen in electrolyte solutions. International Journal of Hydrogen Energy, 43(11): 5551–5560

Lv H, Liu Y, Tang H, Zhang P, Wang J (2017). Synergetic effect of MoS_2 and graphene as cocatalysts for enhanced photocatalytic activity of $BiPO_4$ nanoparticles. Applied Surface Science, 425: 100–106

Matsubara K, Inoue M, Hagiwara H, Abe T (2019). Photocatalytic water splitting over Pt-loaded TiO_2 (Pt/TiO_2) catalysts prepared by the polygonal barrel-sputtering method. Applied Catalysis B: Environmental, 254: 7–14

Muthukumar H, Gire A, Kumari M, Manickam M (2017). Biogenic synthesis of nano-biomaterial for toxic naphthalene photocatalytic degradation optimization and kinetics studies. International Biodeterioration & Biodegradation, 119: 587–594

Nowak M, Kauch B, Szperlich P (2009). Determination of energy band gap of nanocrystalline SbSI using diffuse reflectance spectroscopy. Review of Scientific Instruments, 80(4): 046107-046111

Opoku F, Govender K K, van Sittert C G C E, Govender P P (2017). Understanding the mechanism of enhanced charge separation and visible light photocatalytic activity of modified wurtzite ZnO with nanoclusters of ZnS and graphene oxide: From a hybrid density functional study. New Journal of Chemistry, 41(16): 8140–8155

Peng K, Wang H, Li X, Wang J, Xu L, Gao H, Niu M, Ma M, Yang J (2019). One-step hydrothermal growth of MoS_2 nanosheets/CdS nanoparticles heterostructures on montmorillonite for enhanced visible light photocatalytic activity. Applied Clay Science, 175: 86–93

Sharma S, Pai M. R, Kaur G, Divya, Satsangi R. V,Dass S, Shrivastav R (2019). Efficient hydrogen generation on CuO core/Ag/TiO_2 shell nano-hetero-structures by photocatalytic splitting of water. Renewable Energy, 136: 1202–1216

Shi W, Guo F, Li M, Shi Y, Shi M, Yan C (2019). Constructing 3D submicrometer CoO octahedrons packed with layered MoS_2 shell for boosting photocatalytic overall water splitting activity. Applied Surface Science, 473: 928–933

Tian J, Shao Q, Zhao J, Pan D, Dong M, Jia C, Ding T, Wu T, Guo Z (2019). Microwave solvothermal carboxymethyl chitosan templated synthesis of TiO_2/ZrO_2 composites toward enhanced photocatalytic degradation of Rhodamine B. Journal of Colloid and Interface Science, 541: 18–29

Wang B, Zhang J, Huang F (2017a). Enhanced visible light photocatalytic H_2 evolution of metal-free g-C_3N_4/SiC heterostructured photocatalysts. Applied Surface Science, 391: 449–456

Wang D, Guo Z, Peng Y, Yuan W (2015). A simple route to significant enhancement of photocatalytic water oxidation on $BiVO_4$ by heterojunction with SiC. Chemical Engineering Journal, 281: 102–108

Wang D, Wang W, Wang Q, Guo Z, Yuan W (2017b). Spatial separation of Pt and IrO_2 cocatalysts on SiC surface for enhanced photocatalysis. Materials Letters, 201: 114–117

Wang Y, Zhang F, Yang M, Wang Z, Ren Y, Cui J, Zhao Y, Du J, Li K, Wang W, Kang D J (2019). Synthesis of porous MoS_2/CdSe/TiO_2 photoanodes for photoelectrochemical water splitting. Microporous and Mesoporous Materials, 284: 403–409

Yan H, Yang J, Ma G, Wu G, Zong X, Lei Z, Shi J, Li C (2009). Visible-light-driven hydrogen production with extremely high quantum efficiency on Pt–PdS/CdS photocatalyst. Journal of Catalysis, 266(2): 165–168

Yan X, Ye K, Zhang T, Xue C, Zhang D, Ma C, Wei J, Yang G (2017). Formation of three-dimensionally ordered macroporous TiO_2@nanosheet SnS_2 heterojunctions for exceptional visible-light driven photocatalytic activity. New Journal of Chemistry, 41(16): 8482–8489

Yin X, Li L, Jiang W, Zhang Y, Zhang X, Wan L, Hu J (2016). MoS_2/CdS nanosheets-on-nanorod heterostructure for highly efficient photocatalytic H_2 generation under visible light irradiation. ACS Applied Materials & Interfaces, 8(24): 15258–15266

Yu X, Kou S, Zhang J, Tang X, Yang Q, Yao B (2018). Preparation and characterization of Cu_2O nano-particles and their photocatalytic degradation of fluroxypyr. Environmental Technology, 39(22): 2967–2976

Yuan J, Wen J, Zhong Y, Li X, Fang Y, Zhang S, Liu W (2015). Enhanced photocatalytic H_2 evolution over noble-metal-free NiS

cocatalyst modified CdS nanorods/g-C_3N_4 heterojunctions. Journal of Materials Chemistry. A, Materials for Energy and Sustainability, 3(35): 18244–18255

Yuan R, Zhou B, Hua D, Shi C, Li M (2014). Effect of metal-ion doping on the characteristics and photocatalytic activity of TiO_2 nanotubes for the removal of toluene from water. Water Science & Technology A Journal of the International Association on Water Pollution Research, 69(8): 1697–1704

Zhang G, Zhang W, Wang P, Minakata D, Chen Y, Crittenden J (2013). Stability of an H_2-producing photocatalyst (Ru/$(CuAg)_{0.15}In_{0.3}Zn_{1.4}S_2$) in aqueous solution under visible light irradiation. International Journal of Hydrogen Energy, 38(3): 1286–1296

Zhang X, Zhao J, Guo L (2014). Band gap-tunable $(CuAg)_xIn_{2x}Zn_{2(1-2x)}S_2$ solid solutions synthesized by hydrothermal method with ultrasonic assistance and their photocatalytic H_2 production performance. Journal of Alloys and Compounds, 582: 617–622 doi:10.1016/j.jallcom.2013.08.071

Zhang Y, Li H, Zhang Y, Song F, Cao X, Lyu X, Zhang Y, Crittenden J (2018). Statistical optimization and batch studies on adsorption of phosphate using Al-eggshell. Adsorption Science and Technology, 36(3–4): 999–1017

Zhang Y, Zhang Y, Li X, Dai J, Song F, Cao X, Lyu X, Crittenden J C (2019). Enhanced photocatalytic activity of SiC-based ternary graphene materials: A DFT study and the photocatalytic mechanism. ACS Omega, 4(23): 20142–20151

Zhao H, Mu X, Yang G, George M, Cao P, Fanady B, Rong S, Gao X, Wu T (2017). Graphene-like MoS_2 containing adsorbents for Hg^0 capture at coal-fired power plants. Applied Energy, 207: 254–264

Zhao J, Ge S, Pan D, Shao Q, Lin J, Wang Z, Hu Z, Wu T, Guo Z (2018). Solvothermal synthesis, characterization and photocatalytic property of zirconium dioxide doped titanium dioxide spinous hollow microspheres with sunflower pollen as bio-templates. Journal of Colloid and Interface Science, 529: 111–121

Zhao W, Feng Y, Huang H, Zhou P, Li J, Zhang L, Dai B, Xu J, Zhu F, Sheng N, Leung D Y C (2019). A novel Z-scheme Ag_3VO_4/$BiVO_4$ heterojunction photocatalyst: Study on the excellent photocatalytic performance and photocatalytic mechanism. Applied Catalysis B: Environmental, 245: 448–458

Zhou F, Yan C, Liang T, Sun Q, Wang H (2018). Photocatalytic degradation of orange G using sepiolite-TiO_2 nanocomposites: Optimization of physicochemical parameters and kinetics studies. Chemical Engineering Science, 183: 231–239